IIETA International Information and Engineering Technology Association
Advancing the World of Information and Engineering

Enhancement of Mechanical Properties of PMMA Reinforced with a Composite of $Bi_2O_3:Fe_2O_3$ for Radiation Application

Saleem Mohammad Mahmood[1*] , Mahdi M. Mutter[2] , Ali K. Aobaid[1]

[1] Department of Physics, College of Education for Pure Science, University of Anbar, Anbar 31001, Iraq
[2] Center of Apply Physics, Ministry of Science and Technology, Baghdad 10011, Iraq

Corresponding Author Email: sel20u3009@uoanbar.edu.iq

ABSTRACT

This investigation aimed to improve the mechanical and radiation shielding capabilities of polymethyl methacrylate (PMMA) by incorporating a ($Bi_2O_3:Fe_2O_3$) nanoparticulate composite. Doping levels were systematically varied at weight percentages of 0.5%, 1%, 3%, and 5%. Comprehensive analyses, including tensile strength, strain, hardness, structural, and morphological evaluations, were conducted. The structural transformation of PMMA was confirmed by X-ray diffraction, revealing a cubic phase post-doping. Scanning electron microscopy (SEM) images elucidated a range of crystalline sizes upon nanoparticle integration. Mechanical property assessments indicated a significant enhancement in tensile strength, which escalated from 5.45 MPa in the undoped matrix to 14.85 MPa at the highest doping concentration. However, the distribution of stress within the PMMA:($Bi_2O_3:Fe_2O_3$) composites was observed to be non-uniform. Furthermore, the impact strength demonstrated a marked increase in the specimens containing 0.5% and 1% wt. of ($Bi_2O_3:Fe_2O_3$), suggesting an optimal doping threshold for impact resistance. Shore D hardness measurements also reflected this trend of improvement, with values rising from 71.6 in the pure PMMA to 89 in the composites as the doping ratio increased. Collectively, these findings underscore the potential of ($Bi_2O_3:Fe_2O_3$) nanoparticles to fortify PMMA matrices, offering promising avenues for the development of advanced materials with tailored properties for protective applications against ionizing radiation.

1. INTRODUCTION

The relentless pursuit of polymer innovation and enhancement is a cornerstone of contemporary research efforts, attracting significant attention across diverse industrial sectors [1-4]. Prominent among these materials is polymethyl methacrylate (PMMA), a thermoplastic polymer distinguished by its transparency, durability, and rigidity. PMMA's versatile applications span across industries, serving as the material of choice for products ranging from optical lenses and LED lighting to automotive components and shatter-resistant glass substitutes [5].

The applicability of PMMA extends into the medical field due to its exceptional biocompatibility, ease of processing, and aesthetically pleasing finish, making it a preferred material for dental prostheses, bone cement, and other biomedical devices [6]. Its prominence in denture fabrication is particularly noteworthy, positioning PMMA among the most extensively employed materials in dental applications [7].

In the realm of manufacturing, the blending of polymers has emerged as a pivotal technique for tailoring material properties to achieve optimal performance characteristics. The efficaciousness of polymer blends hinges on the intrinsic properties of the constituents and their spatial arrangement. Compatibility and phase behavior are critical, with high molecular weight polymer blends typically manifesting as two-phase systems characterized by diverse morphologies, including co-continuous structures, lamellar arrangements, and dispersed spherical domains [8].

Compatibilized immiscible blends have been reported to exhibit a synergistic combination of mechanical properties when fabrication and compositional parameters are finely tuned [9-11]. An investigation by Almuqrin et al. [12] explored the impact of incorporating oxides such as Bi_2O_3, PbO, CdO, and B_2O_3 into PMMA. It was observed that substituting Bi_2O_3 for B_2O_3 led to a gradual increase in density from 4.334 to 5.742 g/cm^3. Concurrently, the molar volume (Vm) expanded from 37.197 to 38.429 cm^3/mol as the Bi_2O_3 content rose from 10 to 25 mol%. This addition was accompanied by a reduction in Young's modulus, bulk modulus, shear modulus, and longitudinal modulus, revealing a transition towards a more flexible material capable of withstanding longitudinal deformation preferentially over shear stress.

Building upon this foundation, the present study employed a casting technique to synthesize PMMA composites doped

with (0.5, 1, 3, and 5) wt.% of (Bi_2O_3:Fe_2O_3) for gamma radiation shielding applications. The subsequent sections detail a comprehensive analysis of the mechanical properties of these composites, aiming to elucidate the implications of doping concentrations on PMMA's structural integrity and shielding efficacy.

2. EXPERIMENTAL METHODS

2.1 Materials

PMMA, regularly known as poly (methyl methacrylate), is a chemical compound. It is a 45% styrene-containing, faded-colored, viscous liquid with the additional advantage of getting exceptional mechanical and chemical qualities furnished via Alfa Aesar (Tewksbury, USA). The fillers are (Fe_2O_3, gamma, celebration 99%, (20–40) nm, Sky Spring Nanomaterials, Inc. USA) and (Bi_2O_3, 99.9%, 80 nm, Houston, USA). The filler and resin utilized within the synthesis have been each annular satisfactory. PMMA (Bi_2O_3:Fe_2O_3) composites were made using a casting method. The matrix changed first mixed with finely powdered (Bi_2O_3: Fe_2O_3) at various weight possibilities (0, 0.5, 1, 3, and 5) wt.%. using an electric blender for one hour at a slow pace and then with an ultrasonicator for 5 minutes. After finishing the response procedure with the addition of 0.01 hardener, the electric mixer turned into turned off for five minutes before the samples were prepared in special molds designed for this purpose. The sample is processed in a vacuum oven at 80°C for 6 hours, then left for 24 hours to cool at room temperature. For extra characterization, the samples had been, in the end, sliced into the necessary dimensions.

2.2 Characterization

The structural properties were investigated by using X-ray diffraction (XRD), The XRD dives were made in Siemens Company using a 1.54 °A wavelength. The surface morphology analysis by using Scanning Electron Microscopy (SEM), type JEOL.JSM-67001, Germany. An ordinary computerized device from Jinan Shijin Group Comp become employed for trying out tensile specimens made according to ASTM trendy D638-87 [13] at an ongoing pressure waft charge of 1 mm/min at the temperature of the room.

Each sample underwent each test 3 times, and the findings are common to the information from the ones 3 assessments. According to ISO-179 [13], the impact takes a look at what was executed at room temperature, and the Time Group Inc.-furnished XJU-22 effect takes a look at equipment employed byan unnotched Charpy. The following connection lets in for the calculation of touch energy:

$$G_c = U_c / A \qquad (1)$$

where Gc is the Impact resistance of the substance J/m². Uc is the strength had to fracture a sample (J). A is the sample's cross-sectional measurement m².

This method may be utilized for figuring out fracture durability:

$$K_c = (G_c)^{1/2} Eb \qquad (2)$$

where: K_c is the sample's fracture resistance (N.M$^{-3/2}$). Gc is the material's resistance to impact (measured in J/m²). Eb is

the substance's Young's modulus (in MPa). The specimens' hardness was determined using the Shore D hardness taken a look at it according to ASTM-D-2240 [13]. The average outcomes of five checks on each pattern were published.

3. RESULTS AND DISCUSSION
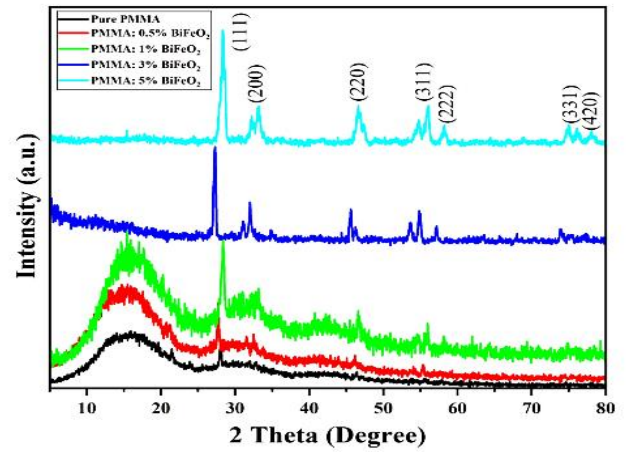
Figure 1. XRD pattern of PMMA: Bi_2O_3:Fe_2O_3) Nanoparticles composite

The XRD spectra of the PMMA: (Bi_2O_3:Fe_2O_3) are shown in Figure 1. The rotation peak was around 28.392°. Figure 1 indicates the amorphous nature of the pure sample (PMMA). This might be attributable to the intermolecular interactions occurring inside the lengthy polymer chain structure's many flaws [14]. The XRD spectra of the PMMA: (Bi_2O_3:Fe_2O_3) reveal various prominent peaks at 28.392°, 32.72°, 46.76°, 54.48°, 55.72°, 74.24° and 76.32° as shown in Figure 1. These peaks are seen to persist in the same location across all samples but the intensity was change. The position of peaks observed is in agreement with the standard (JCPDS card No.00-043-0184). The scattering from polymer layers may be the cause of the additional peaks seen in the samples. The following Table 1 displays the determined values for the crystallite size and strain using Scherrer's formula and the W-H plot, where the Scherrer formula is:

$$D = k\lambda/\beta \cos\theta \qquad (3)$$

where k is a constant (1.5406 oA for CuK) and the wavelength of the employed X-ray radiation is equal to 0.94. The microstrain (ε) may be calculated using the Williamson and Smallman formula [15].

$$\varepsilon = \beta \cos\theta/4 \qquad (4)$$

The crystallite size of the PMMA: (Bi_2O_3:Fe_2O_3) is found in the range (13.318 and 25.831) nm additionally, the strain dropped in the range (1664 to 62)×10^{-4}. The length of the crystallites within the filler particles, as determined using the aforementioned value, does not differ by way of a big quantity. The W-H method's assessment of the effects of strain and crystallite size may result in a small length distinction [16, 17]. The results of crystalline size showed the best sample was PMMA: 3% (Bi_2O_3:Fe_2O_3), in general, the values of crystalline size of other samples were random, and this is due

to inter distance in the crystalline material of the PMMA:(Bi_2O_3:Fe_2O_3) composites.

Table 1. The crystallite size (D) and strain of the PMMA: (Bi_2O_3:Fe_2O_3) composites

Name of Sample	Crystalline Size D (nm)	Strain$\times 10^{-4}$
PMMA	1.784	1644
PMMA: 0.5% (Bi_2O_3:Fe_2O_3)	13.318	119
PMMA: 1% (Bi_2O_3:Fe_2O_3)	6.840	227
PMMA: 3% (Bi_2O_3:Fe_2O_3)	25.831	62
PMMA: 5% (Bi_2O_3:Fe_2O_3)	14.40	108

Figure 2 shows the images of SEM of the surface morphology of PMMA composite with 0 wt.%, 0.5 wt.%, 1 wt.%, 3 wt.%, and 5 wt.% (Bi_2O_3:Fe_2O_3). There are no observable particles on the surface of the pure PMMA composite. However, we observed an even distribution of particles, which dispersed more densely with the increasing loading in the case of the PMMA: (Bi_2O_3:Fe_2O_3) composites [18]. The data of SEM images showed the particle size of all prepared samples were (276.655, 260, 394.67, 312.465, and 551.67) nm of PMMA: (0, 0.5, 1, 3, and 5) wt.% (Bi_2O_3:Fe_2O_3), respectively.

The position of resin to the PMMA within the additive was conglomerate, which brought about the excessive particle length of the additions. Also, the agglomeration of filler particles into larger debris is proven in Figure 2(e) for composites with 5% filler loading, but, and must be reduced for the composites to perform properly [19].
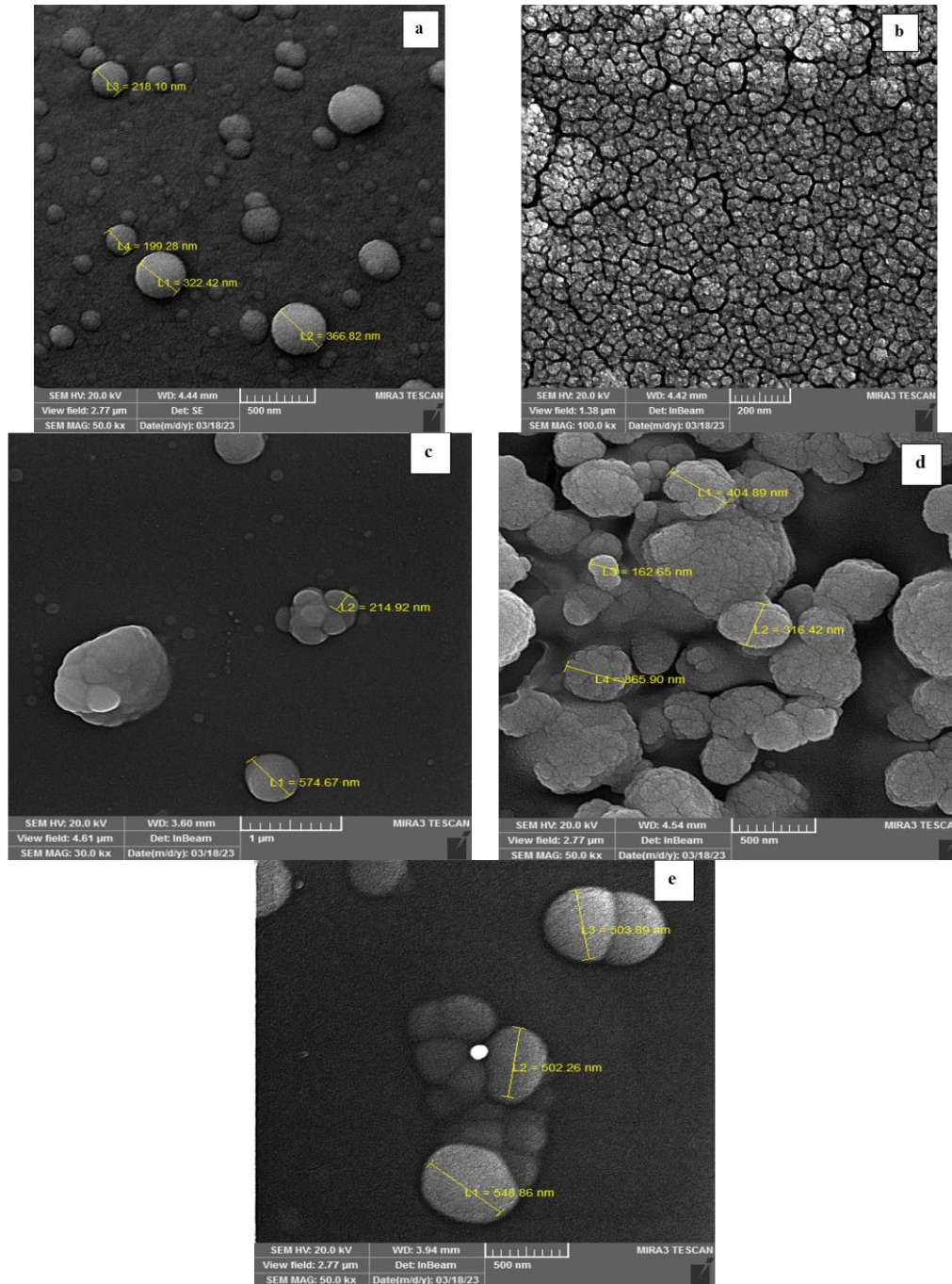
Figure 2. SEM images of PMMA: (Bi_2O_3:Fe_2O_3), (a) PMMA pure, (b) 0.5% (Bi_2O_3:Fe_2O_3), (c) 1% (Bi_2O_3:Fe_2O_3), (d) 3% (Bi_2O_3:Fe_2O_3), (e) 5% (Bi_2O_3:Fe_2O_3)

Figure 3 shows the results of the tensile of the PMMA: $(Bi_2O_3:Fe_2O_3)$ composites. It is clear that the behavior of PMMA changes from soft to hard after composite with $(Bi_2O_3:Fe_2O_3)$. The values of tensile increased from (5.45 to 14.85) MPa with increasing of ratios $(Bi_2O_3:Fe_2O_3)$. The reason for this result due to the increase in stress can be returned to the increase in the ratios of oxides, and their spread among the chains of the polymer led to an increase in stress, and these results are compatible with the results of the researchers [20, 21].
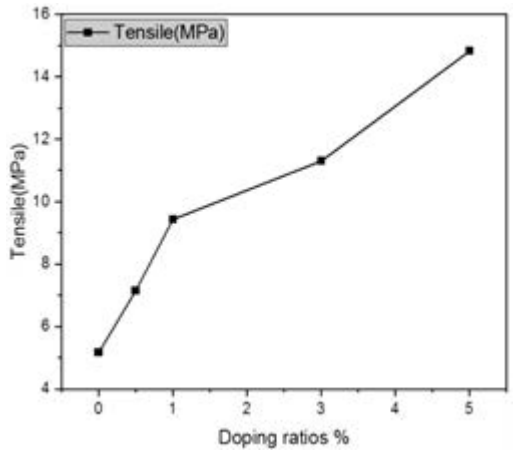
Figure 3. Stress curve of PMMA: $(Bi_2O_3:Fe_2O_3)$

Figure 4 shows the compressibility test results of the PMMA: $(Bi_2O_3:Fe_2O_3)$ composites. In the evaluation of the alternative samples, there has been a much less compressibility test on the 0.5% $(Bi_2O_3:Fe_2O_3)$ sample and a high compressibility test on the sample 5% $(Bi_2O_3:Fe_2O_3)$, where the values of compressibility test increased with increasing the ratios of composites (28.01 to 79.42) MPa. We can see the force of compressibility increased with increasing the ratios of composite oxide. These results can be returned to the good and homogeneous spread of nanoparticles during the polymer chains, which led to an increase in the resistance of the compressibility of prepared samples, these results agree with the results of the study [22].
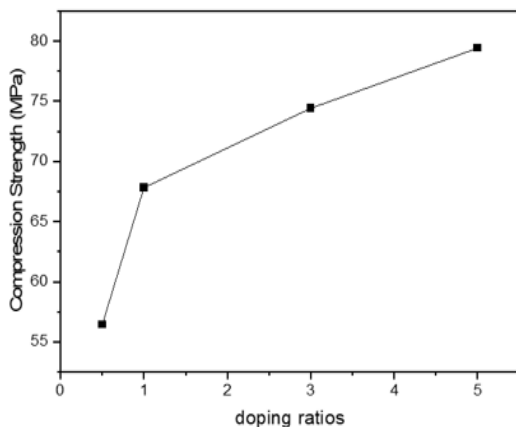
Figure 4. Compressibility test curve of PMMA: $(Bi_2O_3:Fe_2O_3)$

It can be seen from Figure 5 that the values of impact strength for PMMA samples reinforced with particles of $(Bi_2O_3:Fe_2O_3)$. The impact strength values reach the maximum value equal (1.2 KJ/m²) at a weight fraction content of 5%

$(Bi_2O_3:Fe_2O_3)$ as compared with the impact strength value of pure PMMA (reference specimen) which is equal (0.6 KJ/m²). This behavior may be related to the natural powder of composites $(Bi_2O_3:Fe_2O_3)$, these results are due to a good spread of $(Bi_2O_3:Fe_2O_3)$ and homogeneous molecules in the polymer [23-25].

According to the data in Figure 6, PMMA has a shore D hardness of $(Bi_2O_3:Fe_2O_3)$. Doping concentrations have additionally been proven to enhance the shore D hardness values of PMMA :($Bi_2O_3:Fe_2O_3$). It may be explained by an increase in hardness with higher doped $(Bi_2O_3:Fe_2O_3)$ ratios due to great chain entanglements between chains of doped $(Bi_2O_3:Fe_2O_3)$ minerals and chains of nanoparticle-doped PMMA [13]. Measurements of Shore D hardness found increased in values from (71.6 to 89).
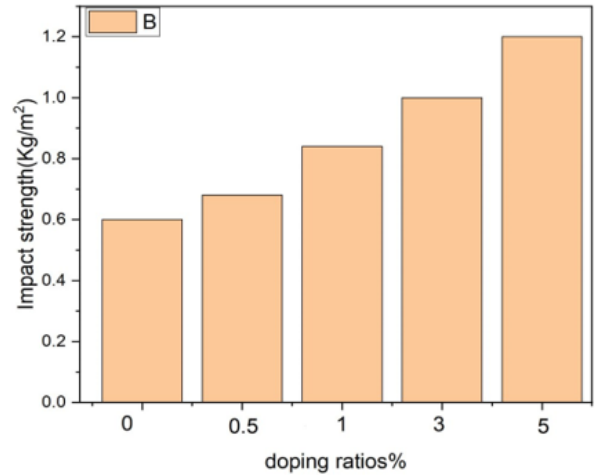
Figure 5. Impact strength for PMMA: $(Bi_2O_3:Fe_2O_3)$
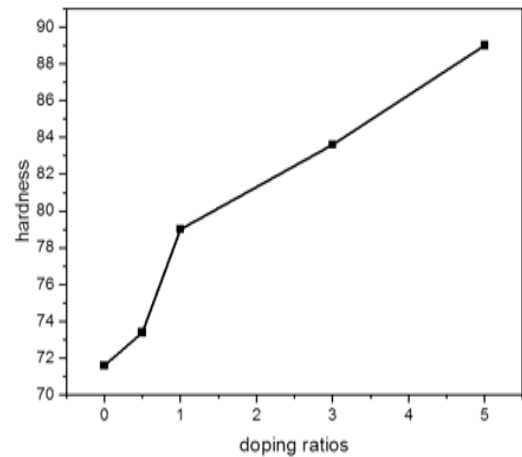
Figure 6. Shore D hardness of PMMA: $(Bi_2O_3:Fe_2O_3)$

4. CONCLUSIONS

In the present work, attempts are made to develop PMMA polymer which is used in many applications. So, the Nanocomposites of $(Bi_2O_3:Fe_2O_3)$ adding to the PMMA at different ratios, and it was concluded the following:
1. The results of the XRD showed that the crystalline size of PMMA was amorphous, but after adding $(Bi_2O_3:Fe_2O_3)$, it was changed to cubic phase and multi-crystalline. The crystalline sizes were (1.78, 13.318, 6.840, 25.831, and 14.40) nm of (0.5, 1, 3, and 5) wt.%. doping, respectively.

Also, strains were $(1644, 119, 227, 62,$ and $108) \times 10^{-4}$.

2. The images of SEM explained the particle size of PMMA: $(Bi_2O_3:Fe_2O_3)$ were $(276.655, 260, 394.67, 312.465,$ and $551.67)$ nm of PMMA: $(0, 0.5, 1, 3,$ and $5)$ wt.% $(Bi_2O_3:Fe_2O_3)$, respectively.

3. The mechanical properties of the PMMA: $(Bi_2O_3:Fe_2O_3)$ such as (hardness, Impact strength, and tensile) were enhanced by increasing the ratios of $(Bi_2O_3:Fe_2O_3)$ doping.

4. The tensile increased from $(5.45$ to $14.85)$ MPa.

5. The results of impact strength increased with increasing of ratios wt. concentration from $(0.6$ to $1.2)$ kg/m^2.

6. The results of shore D hardness increased from $(71.6$ to $80)$ with increasing ratios of doping.

REFERENCES

[1] Truszkiewicz, E., Thalhamer, A., Rossegger, M., Vetter, M., Meier, G., Rossegger, E., Berer, M. (2022). Mechanical behavior of 3D-printed polymeric metamaterials for lightweight applications. Journal of Applied Polymer Science, 139(6): 51618. https://doi.org/10.1002/app.51618

[2] Elshemy, E.A., Showaib, E.A. (2020). Effect of filler loading on erosive characteristics of Epoxy/SiO$_2$ coatings. Solid State Technology, 63(4): 7824-7833.

[3] Alsaab, A.H., Zeghib, S. (2023). Study of prepared lead-free polymer nanocomposites for X-and gamma-ray shielding in healthcare applications. Polymers, 15(9): 2142. https://doi.org/10.3390/polym15092142

[4] Nabhan, A., Ameer, A.K., Rashed, A. (2019). Tribological and mechanical properties of HDPE reinforced by Al2O3 nanoparticles for bearing materials. Int. J. of Advanced Science and Technology, 28(18): 481-489.

[5] Mendoza-Castellanos, J.L., Pantoja-Espinoza, J.C., Rodríguez-Pacheco, L.C., Paraguay-Delgado, F. (2023). Synthesis of PMMA microspheres with tunable diameters: evaluation as a template in the synthesis of tin oxide coatings. Polymers, 15(11): 2419. https://doi.org/10.3390/polym15112419

[6] Issa, S.A., Ahmad, M., Tekin, H.O., Saddeek, Y.B., Sayyed, M.I. (2019). Effect of Bi2O3 content on mechanical and nuclear radiation shielding properties of Bi2O3-MoO3-B2O3-SiO2-Na2O-Fe2O3 glass system. Results in Physics, 13: 102165. https://doi.org/10.1016/j.rinp.2019.102165

[7] Mutluay, M.M., Ruyter, I.E. (2005). Evaluation of adhesion of chairside hard relining materials to denture base polymers. The Journal of prosthetic dentistry, 94(5): 445-452. https://doi.org/10.1016/j.prosdent.2005.08.011

[8] Fang, M., Cot, D., Montoro, C., Semsarilar, M. (2023). A systematic study of a polymer-assisted carboxylate-based MOF synthesis: multiple roles of core cross-linked PMAA-b-PMMA nanoparticles. Polymer Chemistry, 14(5): 662-669. https://doi.org/10.1039/D2PY01202B

[9] Petronyuk, J.S., Priadilova, O.V., Levin, V.M., Ledneva, O.A., Popov, A.A. (2003). Structure and elastic properties of immiscible LDPE-PP blends: dependence on composition. In Materials Research Society Symposium Proceedings, 740: 261-266.

[10] Dhoble, A., Kulshreshtha, B., Ramaswami, S., Zumbrunnen, D.A. (2005). Mechanical properties of PP-LDPE blends with novel morphologies produced with a continuous chaotic advection blender. Polymer, 46(7): 2244-2256. https://doi.org/10.1016/j.polymer.2005.01.057

[11] Chen, J.H., Zhong, J.C., Cai, Y.H., Su, W.B., Yang, Y.B. (2007). Morphology and thermal properties in the binary blends of poly (propylene-co-ethylene) copolymer and isotactic polypropylene with polyethylene. Polymer, 48(10): 2946-2957. https://doi.org/10.1016/j.polymer.2007.03.037

[12] Almuqrin, A.H., Kumar, A., Prabhu, N.S., Jecong, J.F.M., Kamath, S.D., Abu Al-Sayyed, M.I. (2022). Mechanical and gamma-ray shielding examinations of Bi2O3–PbO–CdO–B2O3 glass system. Open Chemistry, 20(1): 808-815. https://doi.org/10.1515/chem-2022-0195

[13] Smith, W.F., Hashemi, J. (2006). Foundations of materials science and engineering. Mcgraw-Hill Publishing.

[14] Hemalatha, K.S., Rukmani, K., Suriyamurthy, N., Nagabhushana, B.M. (2014). Synthesis, characterization and optical properties of hybrid PVA–ZnO nanocomposite: a composition dependent study. Materials Research Bulletin, 51: 438-446. https://doi.org/10.1016/j.materresbull.2013.12.055

[15] Zhou, L., Hu, X., Wu, S. (2013). Effects of deposition temperature on the performance of CdS films with chemical bath deposition. Surface and Coatings Technology, 228: S171-S174. https://doi.org/10.1016/j.surfcoat.2012.06.047

[16] Rameshkumar, C., Sarojini, S., Naresh, K., Subalakshmi, R. (2017). Preparation and characterization of pristine PMMA and PVDF thin film using solution casting process for optoelectronic devices. Jump To References Section, 33(1-2): 12-18. https://doi.org/10.18311/jsst/2017/6215

[17] Choudhury, N., Sarma, B.K. (2009). Structural characterization of lead sulfide thin films by means of X-ray line profile analysis. Bulletin of Materials Science, 32: 43-47. https://doi.org/10.1007/s12034-009-0007

[18] Harish, V., Nagaiah, N., Prabhu, T.N., Varughese, K.T. (2009). Preparation and characterization of lead monoxide filled unsaturated polyester based polymer composites for gamma radiation shielding applications. Journal of Applied Polymer Science, 112(3): 1503-1508. https://doi.org/10.1002/app.29633

[19] Ambika, M.R., Nagaiah, N., Harish, V., Lokanath, N.K., Sridhar, M.A., Renukappa, N.M., Suman, S.K. (2017). Preparation and characterisation of Isophthalic-Bi2O3 polymer composite gamma radiation shields. Radiation Physics and Chemistry, 130: 351-358. https://doi.org/10.1016/j.radphyschem.2016.09.022

[20] Jassim, N., Ahmed, F., Hilal, R. (2015). Charpy impact test for SiO2 nanoparticles/ epoxy composites. Int. J. Sci. Res, 6: 4623-0462.

[21] Salih, S.I., Oleiwi, J.K., Mohamed, A.S. (2018). Investigation of mechanical properties of PMMA composite reinforced with different types of natural powders. ARPN Journal of Engineering and Applied Sciences, 13(22): 8889-8900.

[22] Jassim, N., Farhan, A.J., Hilal, R. (2015). Charpy impact test for SiO2 (nano-micro) particles/epoxy composites. International Research Journal of Engineering and Technology (IRJET), 6: 4623-3628.

[23] Udhayasankar, R., Karthikeyan, B. (2017). Effect of particle loading on flexural properties of coconut shell

reinforced cardanol resin composite. Int Res J Eng Technol IRJET, 4(9): 202-204.

[24] Mahmood, N.Y. (2017). Studying the effect of mixture of pomegranate peel and licorice on the mechanical properties of epoxy. Al-Nahrain Journal for Engineering Sciences, 20(4): 871-875.

[25] Hussain, W.A., Rafiq, S.N. (2012). Mechanical properties of carrot fiber-epoxy composite. Baghdad Science Journal, 9(2): 335-340.